Research Square

Preprints are preliminary reports that have not undergone peer review.
They should not be considered conclusive, used to inform clinical practice,
or referenced by the media as validated information.

Thermodynamic Analysis of a Two-Stage Selective Carbothermic Reduction Process for Deep-Sea Polymetallic Nodules: Part II. Ferromanganese–Silicide Alloy Production

Omid Marzoughi

om17@queensu.ca

Queen's University

Dulmini Hissalle

Queen's University

Christopher Pickles

Queen's University

Research Article

Keywords: Deep-sea polymetallic nodules, manganese-rich residue, selective carbothermic reduction, ferromanganese–silicide alloy, thermodynamic modelling, HSC Chemistry

Posted Date: November 20th, 2026

DOI: https://doi.org/10.21203/rs.3.rs-11292196/v1

License: This work is licensed under a Creative Commons Attribution 4.0 International License.
Read Full License

Additional Declarations: No competing interests reported.

Thermodynamic Analysis of a Two-Stage Selective Carbothermic Reduction Process for Deep-Sea Polymetallic Nodules: Part II. Ferromanganese–Silicide Alloy Production

O. Marzoughi, D. Hissalle, C. A. Pickles

Robert M. Buchan Department of Mining, Queen's University, Kingston,

Ontario, Canada, K7L 3N6

ABSTRACT

The manganese-rich residue remaining after selective recovery of critical metals from deep-sea polymetallic nodules represents a potential resource for manganese-alloy production. This study presents a thermodynamic analysis of the second stage of a proposed two-stage selective carbothermic reduction process to recover manganese, iron and silicon as a ferromanganese–silicide alloy. Equilibrium calculations were performed using the Equilibrium Composition module of HSC Chemistry® 7.1. The effects of temperature, carbon addition, total pressure, gas atmosphere and residue composition on metal recoveries and alloy composition were evaluated. The results show that manganese reduction requires substantially stronger reducing conditions than those used for selective Cu, Ni and Co recovery, supporting the thermodynamic basis of the two-stage process. A well-defined operating window was identified for high manganese recovery and ferromanganese–silicide alloy formation. The predicted high-temperature reduction behaviour was consistent with published experimental studies, including comparable manganese recoveries and alloy manganese contents. The results demonstrate the potential to convert the Stage I manganese-rich residue into a valuable ferromanganese–silicide alloy, improving overall resource utilization.

Keywords: Deep-sea polymetallic nodules; manganese-rich residue; selective carbothermic reduction; ferromanganese–silicide alloy; thermodynamic modelling; HSC Chemistry

1 Introduction

Deep-sea polymetallic nodules represent one of the world's largest undeveloped manganese resources and also contain substantial quantities of nickel, cobalt and copper [1–3]. In the present research, a two-stage process is investigated for the recovery of the valuable metals from the nodules. In the first stage (Stage I) of the proposed two-stage selective carbothermic reduction process, Cu, Ni and Co are selectively recovered as Alloy I, while manganese reduction is suppressed, leaving a residue enriched in manganese, iron and silica. The residue retains considerable economic value and therefore warrants further processing rather than disposal [4]. Effective utilization of the residue is important for maximizing value recovery, reducing waste generation and improving the overall resource efficiency of the proposed process [1]. The resulting Stage I residue represents a potential feed for producing a ferromanganese–silicide alloy (Alloy II), as manganese is used extensively in ferroalloy production [5]. Manganese is consumed predominantly by the steel industry, mainly in the form of ferromanganese and silicomanganese [6]. In steelmaking, manganese acts as an alloying element, deoxidizer and desulfurizer, while silicon provides additional deoxidizing capacity [7]. The ferroalloys are conventionally produced

by carbothermic smelting in submerged arc furnaces [8]. The higher manganese oxides are first reduced to MnO, however the subsequent reduction of MnO to metallic manganese is more difficult and strongly endothermic, requiring a high temperature, a sufficient carbon activity and a low CO partial pressure [7,9,10]. Silica reduction requires still stronger reducing conditions and is sensitive to temperature, carbon addition and slag chemistry [11]. Consequently, these variables, together with pressure and gas atmosphere composition, govern the manganese and silicon recoveries and the resulting Fe–Mn–Si alloy composition [10,12].

Several pyrometallurgical flowsheets for polymetallic nodules incorporate dewatering as an essential pretreatment step and have demonstrated the feasibility of separating non-ferrous metal recovery from subsequent manganese recovery [13–21]. In these processes, Cu, Ni and Co are first concentrated in an alloy or matte, while most of the manganese remains in an oxide-rich slag or residue [16,22]. A staged smelting–reduction approach has demonstrated that Cu, Ni, Co and Mo can first be recovered in a metallic phase, after which the manganese-rich slag can be subjected to a second reduction step to produce high-carbon ferromanganese which highlights the potential for sequential metal recovery and more comprehensive utilization of the nodule constituents [1]. Carbothermic smelting investigations have likewise shown that selective recovery of Cu, Ni and Co can be achieved while retaining manganese in a slag suitable for subsequent ferromanganese or silicomanganese production. The graphite addition and MnO/SiO_2 ratio were identified as key variables governing slag liquidus temperature, alloy composition and metal–slag separation [11].

Carbon, carbon monoxide, hydrogen and methane have been investigated as reducing agents for manganese-containing ores and polymetallic nodules [17,23–31]. Carbon remains the conventional reductant for high-temperature manganese ferroalloy production, whereas gaseous reductants have been considered for lowering solid-carbon consumption and reducing emissions [17,24,32]. Hydrogen, CO and CH_4 can effectively transform higher manganese oxides to MnO and promote the reduction of Cu, Ni, Co and Fe [9,24]. The pre-reduction of polymetallic nodules using H_2, CH_4 and mixed H_2–CH_4 atmospheres produced metallic Fe, Cu, Ni and Co while MnO remained the dominant manganese-bearing phase. This selectivity is advantageous during the first stage, but stronger reducing conditions are required during the second stage because MnO is considerably more stable [7,33]. Methane can support further reduction under suitable conditions, although methane decomposition, carbon deposition, gas diffusion and sensitivity to CO partial pressure may limit its practical application [7,9,33].

The influence of additives, anthracite dosage, reduction time and temperature on the solid-state reduction of polymetallic nodules has been systematically evaluated through carbothermal reduction, gas–solid co-reduction and kinetic studies [15,26,32]. The addition of CaF_2 enhanced the migration and coalescence of reduced alloy particles by decreasing the surface tension of the metallic phase [15]. Under optimized conditions at 1100 °C, Cu, Co and Ni recoveries of 83.91%, 86.74% and 86.48%, respectively, were reported. Gas–solid co-reduction using hydrogen and carbon-containing pellets has also demonstrated that reduction temperature and the carbon-to-oxygen ratio influence alloy formation, metal-particle aggregation and solid-carbon consumption

[32]. Selective carbothermal reduction studies have further demonstrated the importance of temperature, reductant dosage and residence time in controlling reduction kinetics and metal recovery [26]. However, excessive carbon addition and temperatures above approximately 1225 °C promoted the formation of undesirable manganese carbides, demonstrating the importance of controlling the operating conditions. Fe–Ni–Co–Cu alloy formation was further enhanced through iron oxide addition and control of the carbon-to-oxygen and Mn/Fe ratios [34]. Nevertheless, these studies primarily addressed the recovery of Cu, Ni and Co while retaining manganese in the residue, rather than defining the equilibrium conditions required for subsequent Mn–Fe–Si recovery

Thermodynamic modelling is widely used to examine complex pyrometallurgical systems and predict equilibrium phase assemblages, metal recoveries and alloy compositions [1,10,11,13,35]. For polymetallic nodules, thermodynamic calculations indicate that NiO and CuO are reduced preferentially, followed by CoO and iron oxides as the carbon addition increases; further carbon addition increases iron reduction and consequently dilutes the concentrations of Ni, Co and Cu in the alloy [11]. The MnO/SiO_2 ratio has also been identified as a major factor controlling the primary slag phases and liquidus temperature, whereas FeO and Al_2O_3 generally have smaller effects over the investigated composition ranges. Adjustment of the Mn/Fe ratio through iron oxide addition can modify slag formation and liquidus temperature while promoting the aggregation and separation of Fe–Ni–Co–Cu alloy particles [32]. Thermodynamic comparisons of the reducing agents show that higher manganese oxides can be reduced to MnO by C, CO and H_2, whereas MnO remains stable under H_2- and CO-based reduction and requires substantially stronger reducing conditions for metallization [34]. These differences in oxide stability provide the thermodynamic basis for selectively recovering Cu, Ni, Co and Fe while retaining manganese predominantly as MnO. Previous thermodynamic investigations have shown that Ni, Co, Cu and Fe oxides can be reduced to metallic forms while higher manganese oxides are selectively converted to MnO by controlling temperature and reducing conditions [11,19,34]. The stability of the manganese oxides is strongly affected by pressure and atmospheric composition [10]. Increasing the oxygen partial pressure increases the decomposition temperatures and stabilizes the higher manganese oxides, whereas decreasing the oxygen partial pressure favours the sequential formation of Mn_2O_3, Mn_3O_4 and MnO at progressively lower temperatures. The addition of inert gases or water vapour lowers the oxygen partial pressure, thereby decreasing and broadening the decomposition temperature ranges, while increasing the oxygen concentration raises and narrows these ranges. Consequently, pressure and gas composition can significantly alter the equilibrium phase fields and reduction sequence of manganese oxides.

Despite these advances, the manganese-rich residue produced by selective Stage I reduction has not been systematically evaluated as a feed for a second carbothermic reduction stage. In particular, the equilibrium conditions governing the simultaneous recovery of manganese, iron and silicon into a ferromanganese–silicide alloy remain insufficiently defined. The present study therefore involves the thermodynamic analysis of Stage II using the Equilibrium Composition module of HSC Chemistry® 7.1. The effects of temperature, carbon addition, total pressure, gas atmosphere

and residue composition on the equilibrium compositions of the reduced phase assemblages, elemental recoveries and alloy compositions are systematically investigated. The objective is to establish an equilibrium operating window for producing a ferromanganese–silicide alloy (Alloy II) and thereby improve the overall utilization and value recovery of deep-sea polymetallic nodules. The Stage II predictions were also compared with experimental studies on ferromanganese and silicomanganese production from manganese-rich nodule slags and residues to assess consistency in reduction temperature, manganese recovery, alloy composition and the effects of reductant addition and slag chemistry.

2 Thermodynamic Model

The thermodynamic model employed in the present study was described in detail in Part I. Briefly, equilibrium calculations were performed using the Equilibrium Composition module of HSC Chemistry® 7.1 to investigate the high-temperature carbothermic reduction of the residue remaining after the selective recovery of the critical battery metals Cu, Ni and Co. Equilibrium compositions were determined by minimizing the total Gibbs free energy of the heterogeneous system under specified isothermal and isobaric conditions. The calculations were based on the normalized chemical composition of representative deep-sea polymetallic nodules presented in Table 1.

Table 1 Normalized chemical composition of the polymetallic nodules as used in the model for Stage II.

SiO_2 %	Al_2O_3 %	Fe_2O_3 %	MgO %	CaO %	Na_2O %	MnO %	LOI %	TOTAL %
15.38	4.01	8.34	2.91	2.21	2.09	35.41	29.64	100

Following the first-stage selective reduction, the remaining oxide residue, together with the predetermined carbon addition, was used as the feed for the second-stage calculations. The equilibrium model included all relevant gaseous, oxide and metallic species that could form during reduction, with the species grouped into gas, oxide, alloy and carbon phases. Temperature, carbon addition, atmospheric conditions and nodule composition were systematically varied to establish the thermodynamic operating window for ferromanganese–silicide alloy production. The principal features of the thermodynamic model are summarized in Table 2.

Table 2 Summary of the thermodynamic model.

Parameter	Description
Software	HSC Chemistry® 7.1
Module	Equilibrium Composition
Solution method	Gibbs free-energy minimization

Feed	Residue remaining after Stage I selective reduction
Variables	Temperature, carbon addition, pressure, nitrogen atmosphere and nodule composition
Pressure	1 atm (unless otherwise specified)
Carbon addition	Variable (kmole C per 100 kg nodules)
Assumptions	Closed system, thermodynamic equilibrium, ideal phase behaviour unless activity coefficients were specified
Thermodynamic database	HSC MainDB supplemented with OwnDB modifications described in Part I

The equilibrium calculations assume that the reacting system is closed, all reactions proceed to thermodynamic equilibrium, and species within each phase exhibit ideal (Raoultian) behaviour unless activity coefficient data are available. Activity coefficient data for the Cu–Ni–Co alloy and additional thermodynamic data for the mixed oxide species were incorporated into the OwnDB database, as described in Part I. To account for the solubility of species such as carbon and silicon in Alloy II it was assumed to consist of Fe, Mn, Si and C and the amounts were determined as follows: iron from the amounts of Fe, Fe_3C and FeSi, manganese from the amounts of Mn, Mn_7C_3 and Mn_3Si, silicon from Si, FeSi, Mn_3Si and SiC and finally carbon from Fe_3C, Mn_7C_3 and SiC.

These assumptions provide the thermodynamic limits of the process and enable the identification of the equilibrium operating window for the second-stage reduction. A complete description of the thermodynamic model, database development, activity coefficient treatment and species selection is presented in Part I. Accordingly, the present paper focuses on applying the established thermodynamic framework to determine the equilibrium conditions required for converting the manganese-rich residue into a ferromanganese–silicide alloy (Alloy II) and evaluating the effects of the principal operating variables on the metal recoveries and Alloy II composition.

3 Results and Discussion

3.1 Thermodynamic Basis for the Two-Stage Process

Figure 1 shows the standard-state crossover temperatures for the carbothermic reduction of the oxides of copper, nickel, cobalt, iron, manganese and silicon. These temperatures correspond to the points at which the standard Gibbs free-energy changes for the respective reduction reactions become zero. The crossover temperatures for nickel and cobalt are 435 and 496 °C, respectively, followed by iron at 720 °C. Considerably higher temperatures are required for manganese and silicon, with crossover temperatures of 1402 and 1669 °C, respectively. The substantial difference between the crossover temperatures of Cu, Ni and Co and those of Mn and Si provides the

thermodynamic basis for the proposed two-stage process. Cu, Ni and Co can be selectively reduced during Stage I, while manganese and silicon require the stronger reducing conditions applied during Stage II. These values represent standard-state thermodynamic limits and do not account for reaction kinetics, mass transfer or practical metal–residue separation.

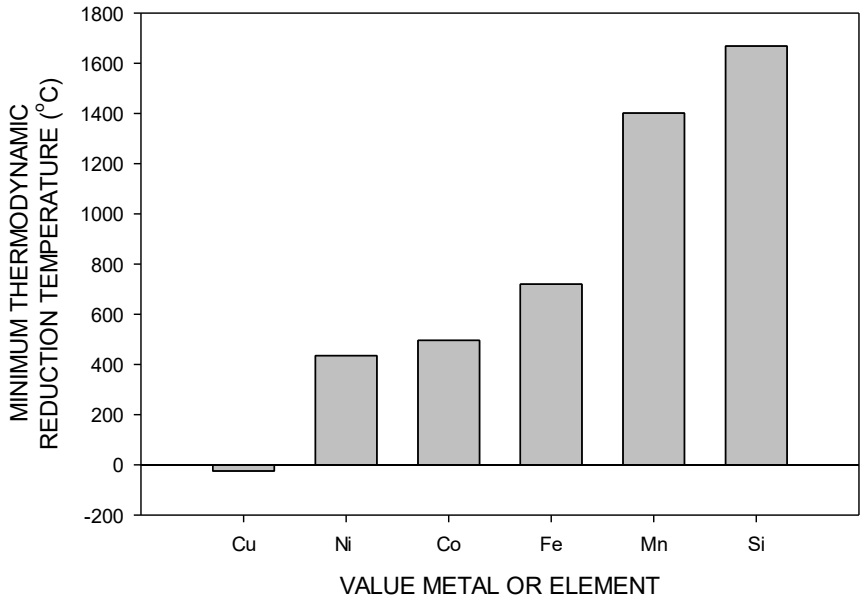

Figure 1 Standard-state crossover temperatures for the carbothermic reduction of the oxides of Cu, Ni, Co, Fe, Mn and Si..

3.2 Thermodynamic Basis for a Two-Stage Selective Carbothermic Process

Part I established that the optimum conditions for the selective reduction of copper, nickel and cobalt occurs within a relatively narrow temperature range centred near 700 to 800 °C, while manganese remains predominantly as manganese(II) oxide (MnO). Consequently, following the recovery of the critical battery metals, the remaining residue still contains significant quantities of manganese oxide together with unreduced iron oxide and silica. The second-stage reduction process involves the carbothermic reduction of MnO and silica (SiO_2) according to the following reactions:

$$\mathrm{MnO_{(s\ or\ l)}} + 2\mathrm{C_{(s)}} = \mathrm{Mn_{(s\ or\ l)}} + 2\mathrm{CO_{(g)}} \qquad (1)$$

$$\mathrm{SiO_{2(s\ or\ l)}} + 2\mathrm{C_{(s)}} = \mathrm{Si_{(s\ or\ l)}} + 2\mathrm{CO_{(g)}} \qquad (2)$$

Any iron that was not recovered during the first-stage selective reduction is also recovered in Alloy II, where it combines with manganese and silicon to produce a ferromanganese-silicide alloy. Figure 2 illustrates the equilibrium distribution of the major metallic elements between Alloy I and Alloy II as a function of temperature for a carbon addition of 0.537 kmole C/100 kg of nodules. The figure shows that the selective recovery of copper, nickel and cobalt is completed at approximately 700 to 800 °C, whereas manganese reduction remains negligible within this temperature range. The amount of iron in Alloy I reaches a maximum near the optimum Stage I

operating temperature before progressively decreasing as iron partitions into Alloy II with increasing temperature. Above approximately 1400 °C, manganese reduction becomes thermodynamically favourable, accompanied by the transfer of iron from Alloy I to Alloy II. The amount of manganese in Alloy II then increases rapidly with temperature before approaching a plateau above approximately 1700 °C. At still higher temperatures, silicon also begins to dissolve in Alloy II, producing a Fe-Mn-Si alloy. The delayed reduction of silicon relative to manganese is consistent with the greater thermodynamic stability of silica and contributes to the progressive enrichment of Alloy II in silicon at the highest temperatures. These results establish the thermodynamic basis for the second reduction stage and demonstrate that high-temperature treatment is required to maximize the recovery of manganese while simultaneously producing a ferromanganese-silicide alloy. They also confirm that the proposed process provides two distinct thermodynamic operating windows: a low-temperature stage for selective recovery of the critical metals followed by a high-temperature stage for recovery of manganese and silicon. The influence of the operating variables governing this second-stage reduction is investigated in the following sections.

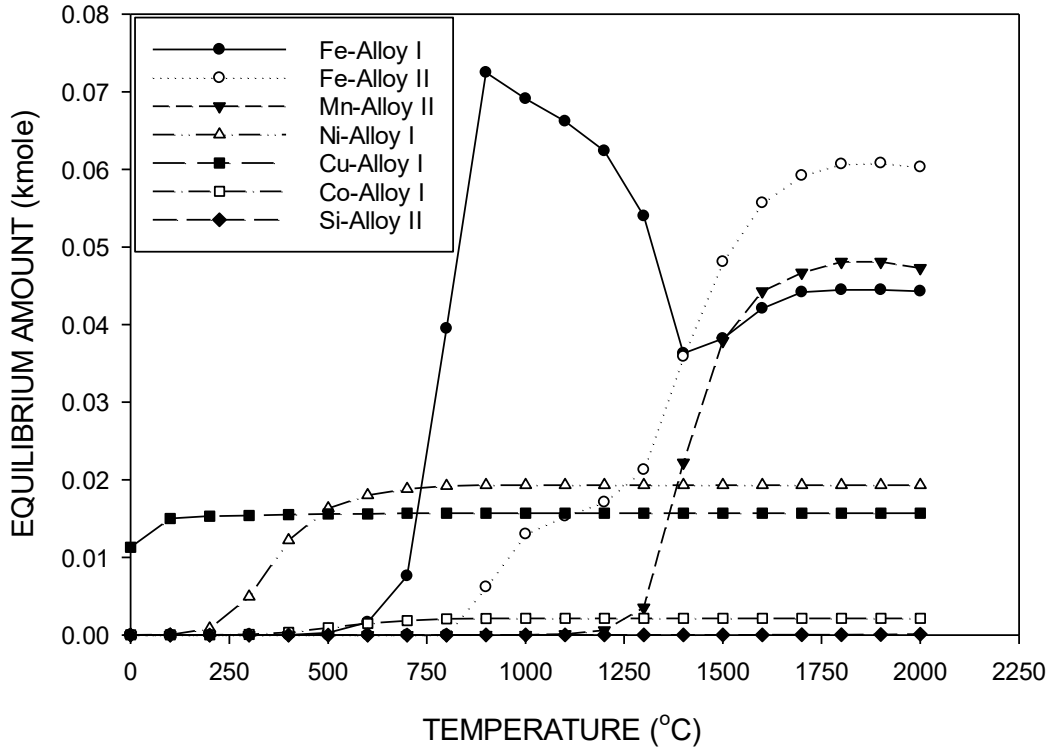

Figure 2 Thermodynamic basis for the second-stage carbothermic reduction of deep-sea polymetallic nodules.

3.3 Stage II - Selective Reduction of Manganese and Silicon - Alloy II

The second stage of the selective reduction process involves the production of a ferromanganese silicide alloy. Here MnO and SiO_2 are reduced to manganese metal and silicon, respectively, which dissolve in the ferroalloy according to the following reactions:

$$MnO_2 + 2C = Mn + 2CO_{(g)} \quad (3)$$

$$SiO_2 + 2C = Si + 2CO_{(g)} \quad (4)$$

Also, the iron oxide that was not recovered as iron in the low-temperature alloy (Alloy I) is recovered in the ferromanganese silicide alloy. The stoichiometric amount of carbon required to reduce the copper, nickel, cobalt, manganese and iron oxides to their respective metals is 1.12 kmole C/100 kg of nodules. Figures 3(a) and (b) show the behaviour of the iron-containing and manganese-containing species, respectively, as a function of temperature up to 2000 °C for this stoichiometric carbon addition.

For iron, the predominant species at room temperature is $MnFe_2O_4$. As the temperature increases, this decomposes and FeO becomes the predominant iron oxide together with a smaller amount of Fe_3O_4. At about 500 °C, magnetite begins to decrease, followed by FeO at about 650 °C. Iron starts to be produced at about 600 °C and Alloy I begins to form. At about 850 °C, iron in Alloy II begins to form, coinciding with the gradual transfer of iron from Alloy I to Alloy II, while some iron carbide (Fe_3C) is also produced. Above approximately 1400 °C, most of the iron has transferred to Alloy II, consistent with the onset of high-temperature manganese reduction.

For manganese, MnO is present at room temperature together with Mn_2SiO_4, $MnFe_2O_4$ and $NaMnO_4$. The amounts of MnO and $(Mn,Ca)SiO_3$ increase with temperature, while the amounts of manganese ferrite and Mn_2SiO_4 decrease, reflecting the progressive decomposition of the mixed manganese-containing phases prior to metallization. Manganese metal begins to be produced in increasing amounts at about 1300 °C, which is significantly higher than the temperature required for iron reduction, and this corresponds to decreases in the amounts of MnO, $(Mn,Ca)SiO_3$, and a continued decrease in Mn_2SiO_4. The amount of $NaMnO_4$ remains essentially constant across the whole temperature range as it is a relatively stable compound. Although the amount of manganese metal increases substantially above approximately 1400 °C, there is still substantial manganese monoxide present at and above 1500 °C. Therefore, the stoichiometric carbon addition of 1.12 kmole C/100 kg does not provide sufficient carbon to reduce this remaining manganese oxide to manganese metal. Consequently, additional carbon is required to achieve high manganese recoveries during the second reduction stage.

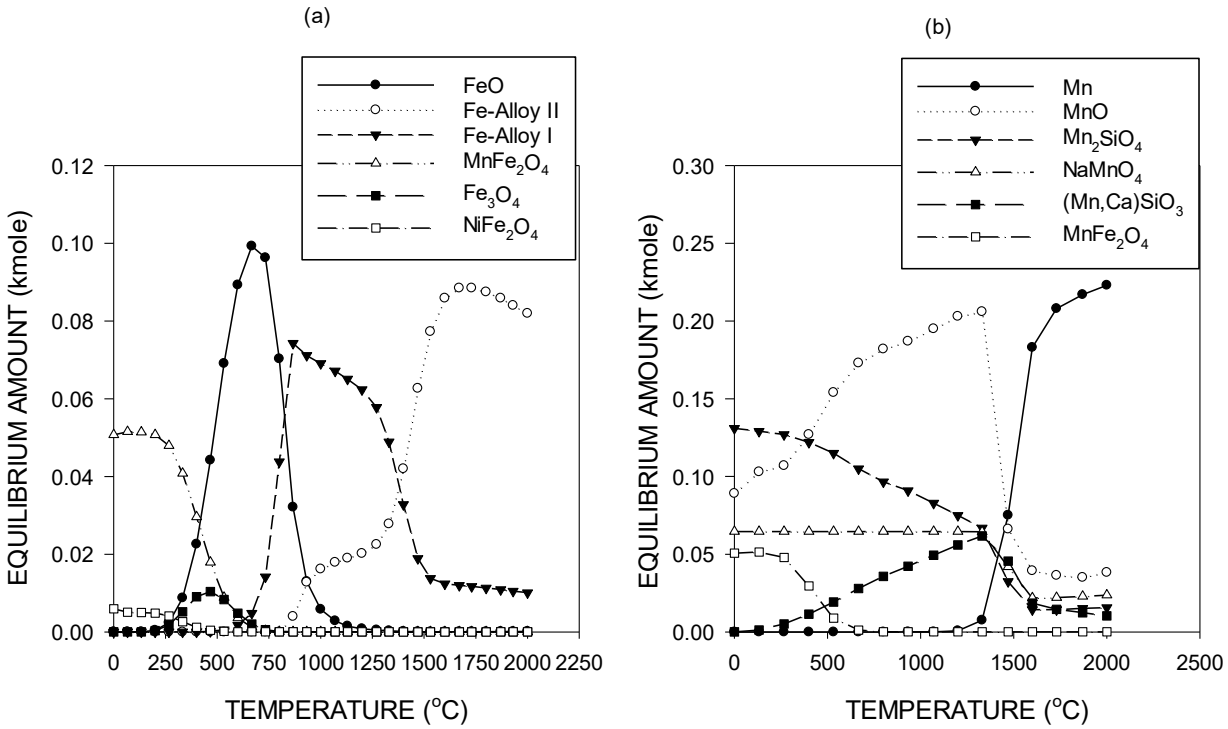

Figure 3 Behaviours of (a) iron-containing and (b) manganese-containing species as a function of temperature for a carbon addition of 1.12 kmole/ 100kg.

Figure 4 shows the changes in the gas composition together with the behaviour of carbon as a function of temperature. From room temperature to about 500 °C, carbon coexists with carbon dioxide and the amount of carbon remains relatively constant. Subsequently, from about 500 °C to 1000 °C, there is a rapid drop in carbon content as the oxides of copper, nickel, cobalt and iron are reduced to their respective metals. During this temperature range, carbon dioxide is progressively converted into carbon monoxide as carbothermic reduction proceeds. The amount of carbon monoxide correspondingly increases, while the amount of carbon dioxide decreases. The carbon dioxide disappears by about 900 °C. From 1000 °C to 1300 °C, there is a slight drop in the carbon content due to the reduction of the remaining iron oxide. During this intermediate temperature range, the carbon monoxide concentration remains approximately constant, indicating relatively limited additional reduction reactions. Above approximately 1300 °C, the amount of carbon drops rapidly and correspondingly the amount of carbon monoxide increases rapidly due to the reduction of manganese monoxide. Carbon is essentially exhausted by approximately 1500 °C, whereas the reduction process is not completed until approximately 1650 °C, with considerable unreduced manganese monoxide still remaining. So, the stoichiometric carbon addition is insufficient to completely reduce manganese oxide and confirms that additional carbon is required to maximize manganese recovery during the second-stage reduction process.

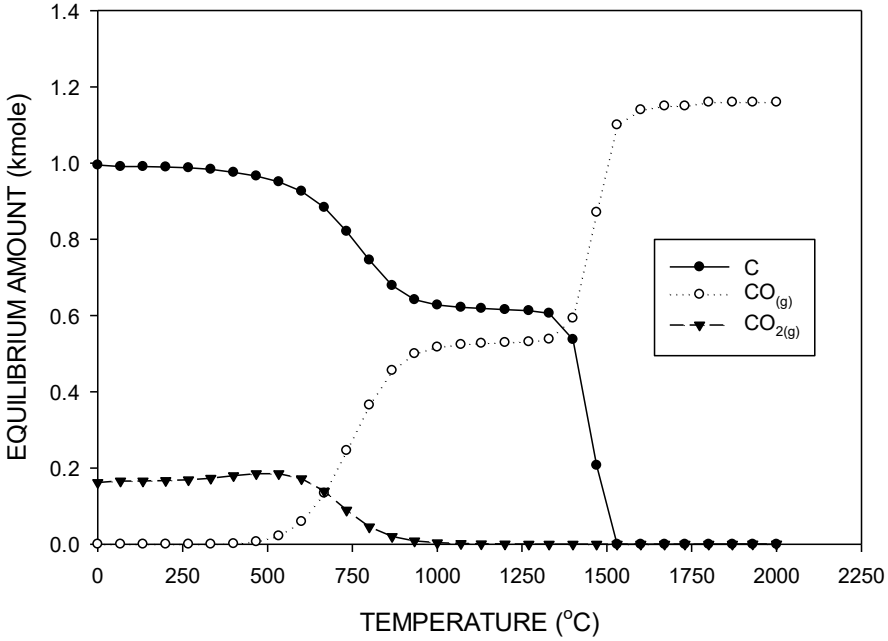

Figure 4 Equilibrium gas composition as a function of temperature for a carbon addition of 1.12 kmole/100 kg.

Figure 5 shows the equilibrium amounts of the solutes in the ferromanganese-silicide alloy as a function of temperature. As discussed previously, these species are utilized in the model to account for both the carbon and the silicon dissolved in the ferromanganese-silicon alloy. From about 850 °C, Fe_3C is produced together with metallic iron, reaching a maximum at approximately 1400 °C and then decreasing. Simultaneously, Mn_7C_3, Mn_3Si, SiC and FeSi start to form. The manganese carbide and silicon carbide quickly reach their maximums and then decrease. In contrast, the amount of ferrosilicon increases continuously with increasing temperature. At about 1650 °C, the amount of manganese silicide begins to decrease, while correspondingly the amount of elemental silicon increases. This indicates that silicon becomes increasingly dissolved in the alloy at the highest temperatures. As the temperature increases, carbides are progressively replaced by silicides and elemental silicon and consequently as the carbon content decreases the silicon content increases. The decrease in the carbide phases at high temperatures is consistent with the progressive depletion of carbon observed in Figure 4. The presence of dissolved carbon in the ferromanganese silicide alloy, together with the carbothermic reduction of silica to silicon, accounts for a substantial proportion of the carbon consumption, thereby limiting the reduction of MnO at the stoichiometric carbon addition. Consequently, additional carbon is required not only to reduce MnO, but also to satisfy the carbon demand associated with carbide formation and silicon production during the second-stage of the reduction process.

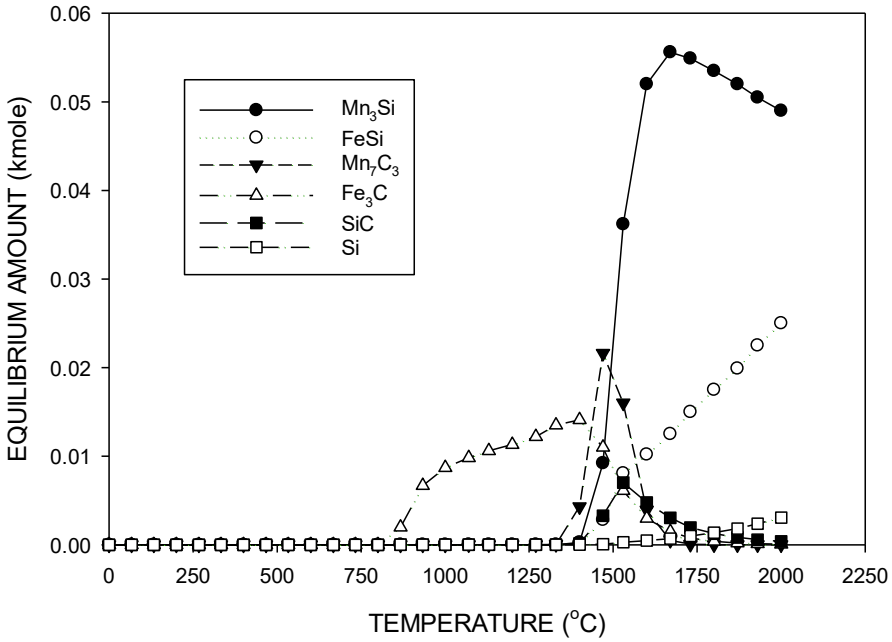

Figure 5 Equilibrium amounts of solutes in Alloy II as a function of temperature for a carbon addition of 1.12 kmole/100 kg.

The above description refers to the complete reduction of the nodules to copper, nickel, iron and manganese. However, for the selective reduction process it is necessary to remove the low-temperature copper-nickel-cobalt-iron alloy. Consequently, for the simulations for Alloy II, the model was modified by excluding the copper-, nickel- and cobalt-containing species that contributed to Alloy I. Furthermore, it was necessary to remove the corresponding amount of iron from the system. Since the objective of the first stage is to produce Alloy I with a high nickel content and the maximum recovery of nickel occurred at 750 °C with a carbon addition of 0.35 kmole C/100 kg, these operating conditions were selected to determine the amount of iron to be removed.

Figure 6 shows the amount of iron produced in Alloy I as a function of carbon addition at 750 °C. The amount of metallic iron increases rapidly between approximately 0.20 and 0.35 kmole C/100 kg before reaching a plateau, indicating that essentially all of the iron reporting to Alloy I has been recovered under these conditions. Here it can be seen that the amount of iron reaches approximately 0.018 kmole at a carbon addition of about 0.35 kmole C/100 kg. Consequently, this amount of iron was subtracted from the initial 0.118 kmole of iron in the feed to give a remaining 0.100 kmole of iron. Therefore, the stoichiometric carbon addition required for the reduction of the remaining manganese and iron oxides to produce a ferromanganese alloy is 1.06 kmole C/100 kg of nodules. An additional 0.49 kmole C/100 kg of carbon is needed to reduce all of the silica to produce a ferromanganese–silicide alloy, giving a total stoichiometric carbon addition of 1.55 kmole C/100 kg. The carbon addition provides the reference stoichiometric requirement for the second stage of the proposed two-stage selective carbothermic process and forms the basis for the

subsequent thermodynamic evaluation of temperature, carbon addition, pressure, gas atmosphere, and residue composition on alloy formation and metal recovery.

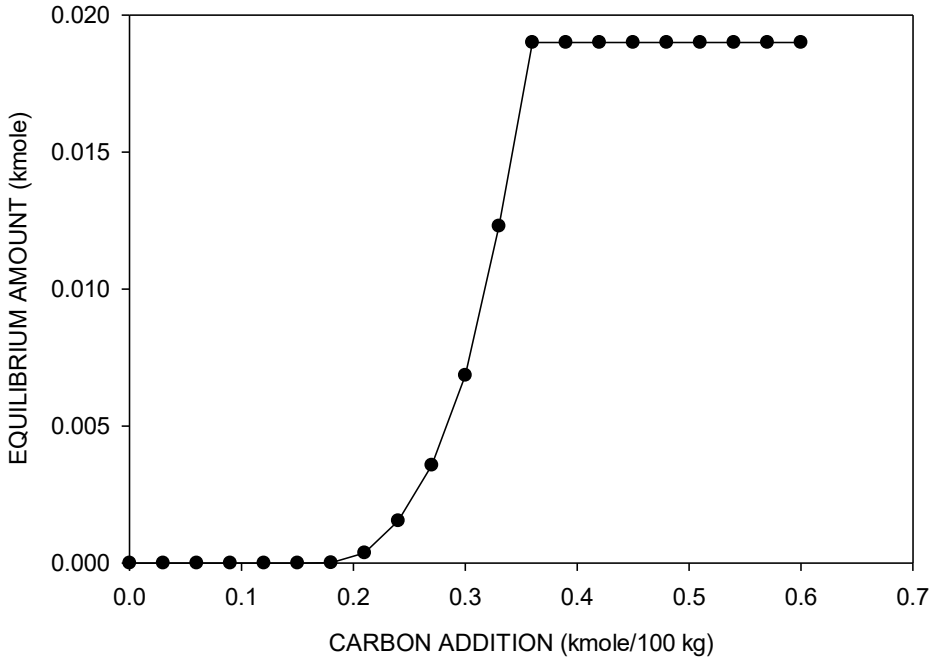

Figure 6 Equilibrium amount of iron in Alloy I as a function of carbon addition at 750 °C.

The equilibrium amounts of the iron-, manganese- and silicon-containing species are shown as a function of carbon addition at 1600 °C in Figures 7(a), (b) and (c). For iron there are only three species, metallic iron, ferrosilicon and iron carbide. The amount of metallic iron decreases slightly with increasing carbon addition, while the amounts of ferrosilicon and Fe_3C increase. The amounts of all three species level off at a carbon addition of approximately 1.42 kmole C/100 kg, indicating that equilibrium has essentially been established above this carbon addition. For Mn, ($(Mn,Ca)SiO_3$, Mn_2SiO_4, $MnSiO_3$), $NaMnO_4$ and MnO are present at low carbon addition, but their amounts decrease with increasing carbon addition. Mn, Mn_3Si and Mn_7C_3 are present across the whole carbon addition range, with their amounts increasing with increasing carbon addition and levelling off at approximately 1.42 kmole C/100 kg. Also, the amount of manganese monoxide levels off and a small amount of residual manganese monoxide remains at high carbon addition. The residual MnO indicates that complete reduction of manganese is not achieved even at 1600 °C under the carbon addition considered**.**

For Si, Mn_3Si and SiC exist across the entire carbon addition range and their amounts also level off at approximately 1.42 kmole C/100 kg. Among the silicon-containing species, Mn_3Si is the predominant phase, whereas SiC is present in relatively small amounts. Additionally, silicates are present over the carbon addition range with their composition changing. For example, as the manganese oxide in the manganese calcium silicates and sodium manganate is reduced, this results in the formation of aluminosilicates and sodium aluminosilicates. Similarly, the amount of

ferrosilicon increases progressively with carbon addition, indicating enhanced silicon dissolution into the ferromanganese alloy as silica reduction proceeds. Therefore, increasing the carbon addition enhances manganese and silicon reduction until equilibrium is reached at approximately 1.42 kmole C/100 kg.

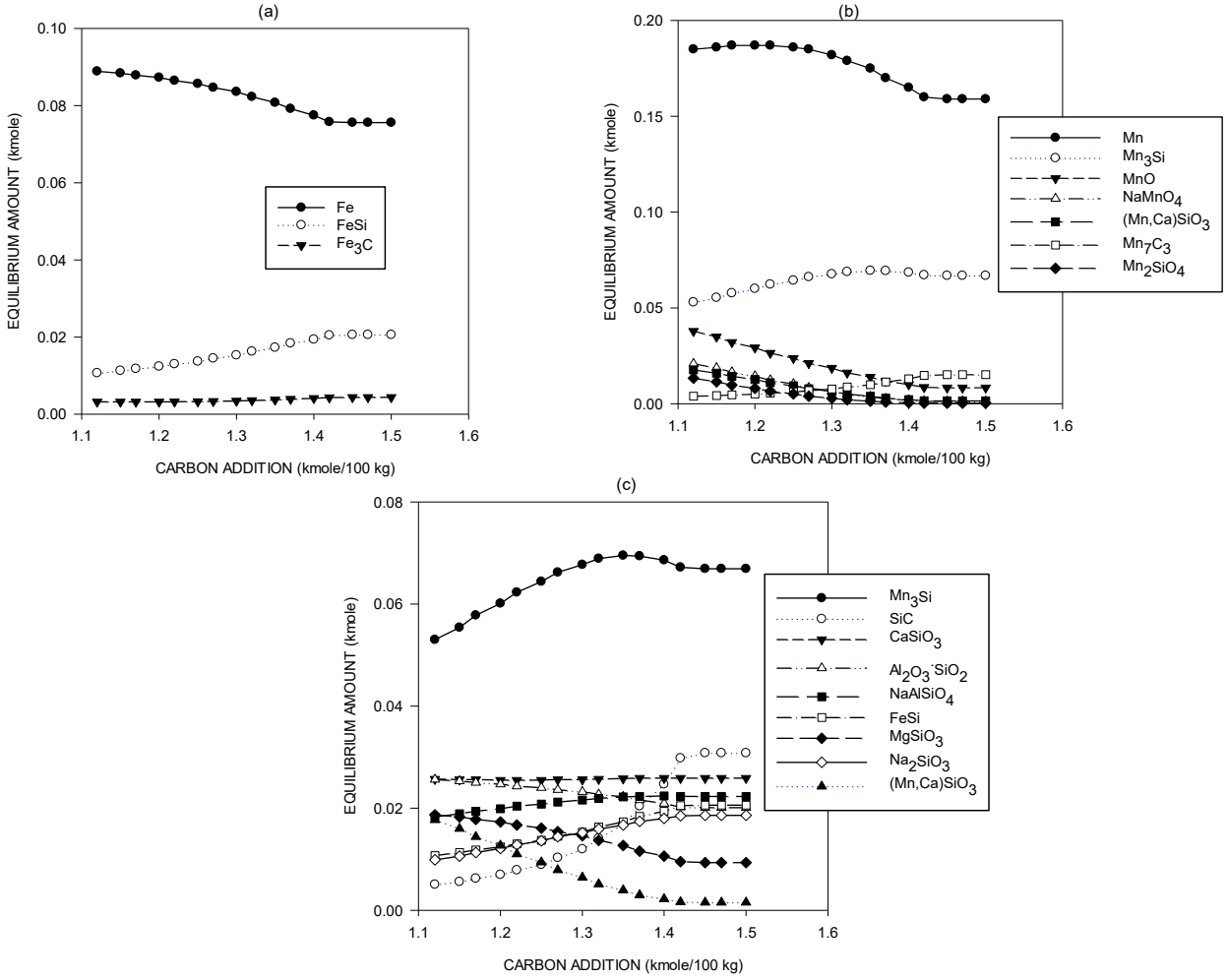

Figure 7 Equilibrium amounts of (a) iron-containing, (b) manganese-containing and (c) silicon-containing species as a function of carbon addition at 1600 °C.

Of particular importance for the production of Alloy II in Stage II is the recovery of manganese into the ferroalloy. In this regard, the amount of MnO is shown between 1000 °C and 2000 °C as a function of carbon addition in Figure 8. At 1000 °C the amount of MnO is relatively high at about 0.20 kmole, and this represents a significant fraction of the total manganese initially present. Subsequently, with increasing temperature, the amount increases slightly due to equilibrium reoxidation over a relatively narrow temperature range immediately prior to the onset of extensive manganese reduction. The majority of the reduction of MnO occurs over a relatively narrow temperature range from about 1450 °C to 1600 °C. The steep decline in the MnO content demonstrates that manganese reduction is highly temperature dependent within this region. Thereafter, for a given carbon addition, the amount of MnO decreases slowly with increasing

temperature. Increasing the carbon addition shifts the equilibrium towards lower residual MnO contents across the entire temperature range investigated. However, even at the highest temperatures and carbon addition considered, some residual MnO remains, demonstrating that complete reduction of MnO is not achieved under these conditions and that further increases in carbon addition or temperature would be required to maximize manganese recovery. The results also confirm that temperature is the dominant operating variable controlling manganese reduction, while carbon addition provides a secondary but beneficial effect by further lowering the equilibrium MnO content.

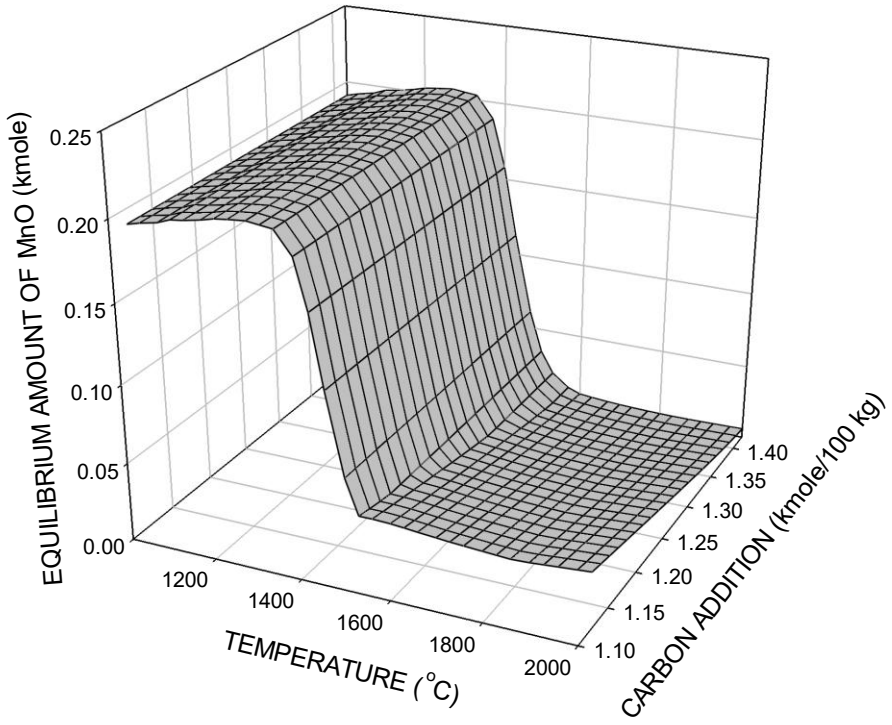

Figure 8 Equilibrium amount of manganese oxide as a function of temperature and carbon addition.

Figures 9(a) and (b) show the effect of temperature for a carbon addition of 1.12 kmole C/100 kg on the recoveries of manganese, iron and silicon and the ferroalloy composition, respectively. The iron recovery was about 95% at 1000 °C and then increased to almost 100% at higher temperatures. Manganese reduction began at about 1200 °C and thereafter the recovery increased slowly and then rapidly to about 72% at 1500 °C. Subsequently, the manganese recovery increased slowly to about 79% at approximately 1850 °C, reflecting the progressive reduction of the remaining MnO at elevated temperatures. Silicon began to be produced at approximately 1400 °C and its recovery then increased rapidly to about 30% at approximately 1700 °C, after which it approached a plateau.

With regards to the ferroalloy composition, at low temperatures the alloy consists predominantly of iron together with carbide phases. As manganese began to be recovered at about 1200 °C, the manganese content of the alloy increased and the iron content decreased. As silica was reduced at approximately 1400 °C, the silicon content of the alloy increased and the carbon content decreased. The most significant changes in alloy composition therefore occur over the same temperature range in which manganese reduction becomes thermodynamically favourable. The ferroalloy composition at 1600 °C was approximately 70% Mn, 22% Fe, 6.7% C and 1.8% Si. Above approximately 1600 °C, both the metal recoveries and alloy composition change only gradually, indicating that equilibrium has largely been established for the stoichiometric carbon addition. However, the manganese recovery remains below 80%, demonstrating that the stoichiometric carbon addition is insufficient to achieve complete manganese reduction despite the high operating temperature.

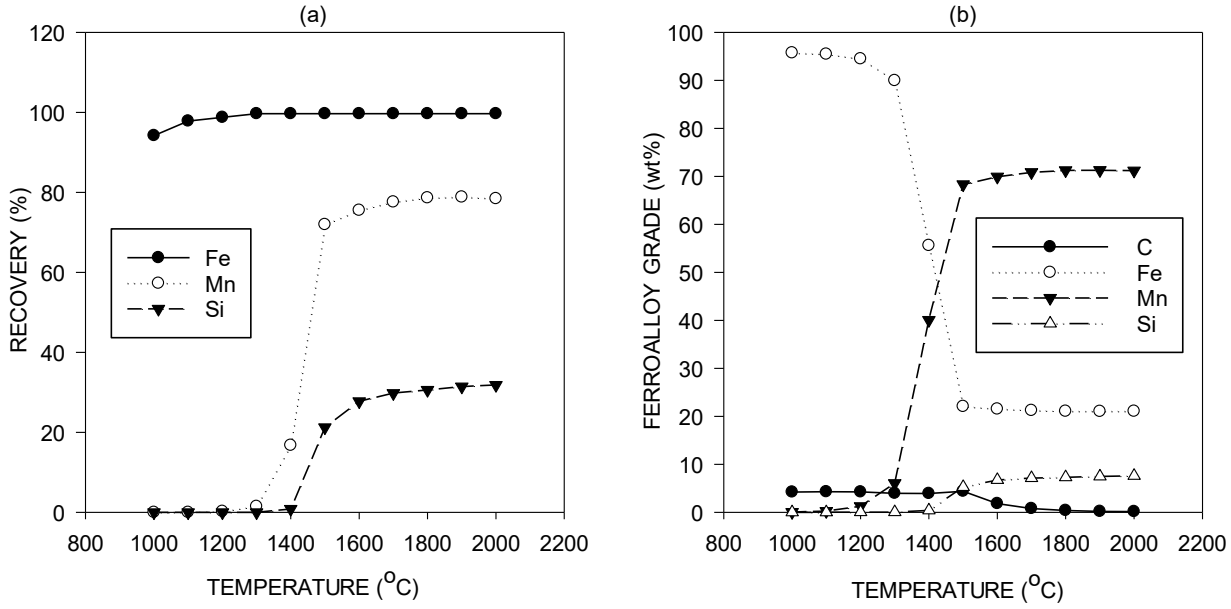

Figure 9 (a) Recoveries of iron, manganese and silicon to Alloy II and (b) the grade of Alloy II as a function of temperature at a carbon addition of 1.12 kmole/100 kg

The effects of carbon addition on the recoveries of manganese, iron and silicon at 1600 °C and the ferroalloy composition are shown in Figures 10(a) and (b), respectively. The carbon addition was varied from 1.12 to 1.62 kmole C/100 kg, which correspond to the stoichiometric requirements for the reduction of the manganese oxide plus iron oxide and the reduction of the manganese oxide plus iron oxide plus silica, respectively. The iron recovery was close to 100% over the whole range of carbon addition. Both the manganese and silicon recoveries increased at about the same rate with increasing carbon addition but then began to level off at a carbon addition of approximately 1.55 kmole C/100 kg. The manganese recovery increased from approximately 75% to about 98%, while the silicon recovery increased from approximately 28% to about 56% over the carbon addition range investigated. With regards to the ferroalloy composition, the composition remained relatively constant, despite the significant increases in manganese and silicon recoveries, reflecting

the above-mentioned recovery trends. The manganese and iron contents decreased slightly at high carbon addition, while the carbon and silicon contents increased. The slight decreases in the manganese and iron contents can be attributed to the increased recovery of silicon and carbon. Consequently, increasing carbon addition produces a gradual shift from a ferromanganese alloy towards a ferromanganese–silicide alloy. The alloy composition for a carbon addition of 1.62 kmole C/100 kg was approximately 69% Mn, 16.3% Fe, 5% C and 10.2% Si. Hyperstoichiometric carbon addition are therefore required to maximize manganese recovery while simultaneously increasing silicon recovery through the continued reduction of SiO_2. Beyond approximately 1.55 kmole C/100 kg, however, further carbon addition provide only minor improvements in both metal recoveries and alloy composition.

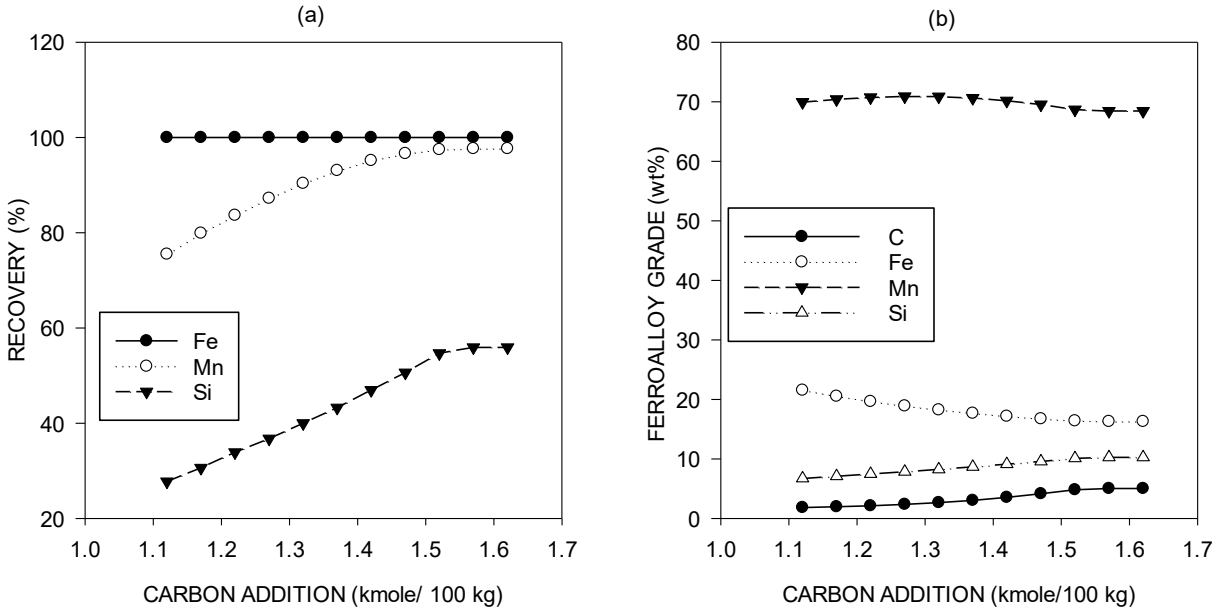

Figure 10 (a) Recoveries of iron, manganese and silicon to Alloy II and (b) the grade of Alloy II as a function of carbon addition at 1600 °C.

Figures 11(a) and (b) show the recoveries of manganese, iron and silicon in the ferroalloy and the ferroalloy composition, respectively, as a function of atmospheric pressure, and Figures 12(a) and (b) show the corresponding recoveries and compositions, respectively, as a function of the amount of nitrogen added for a carbon addition of 1.12 kmole C/100 kg at 1600 °C. For both atmospheric conditions, the recoveries of manganese and silicon increased only slightly with decreasing pressure and increasing nitrogen addition because the reduced partial pressure of carbon monoxide promotes the reduction reactions. According to Le Chatelier's principle, lowering the carbon monoxide partial pressure shifts the equilibrium towards the reduction reaction products. The iron recovery remained constant as it was essentially completely recovered at 1600 °C.

With regards to the ferroalloy composition, the amounts of manganese and silicon increased slightly with decreasing pressure and similarly with increasing nitrogen addition, while the iron content was essentially constant. The carbon content also changed only marginally over the

pressure range investigated. For both cases involving changes in the atmospheric conditions, the gas phase consists predominantly of carbon monoxide and therefore the reductions in the partial pressure of carbon monoxide due to the decrease in total atmospheric pressure or the addition of nitrogen are relatively small. Thus, there is only a small increase in the metal recoveries. Therefore, the pressure and nitrogen atmosphere have only minor effects on the second-stage reduction process and are unlikely to provide significant practical advantages for ferromanganese-silicide alloy production.

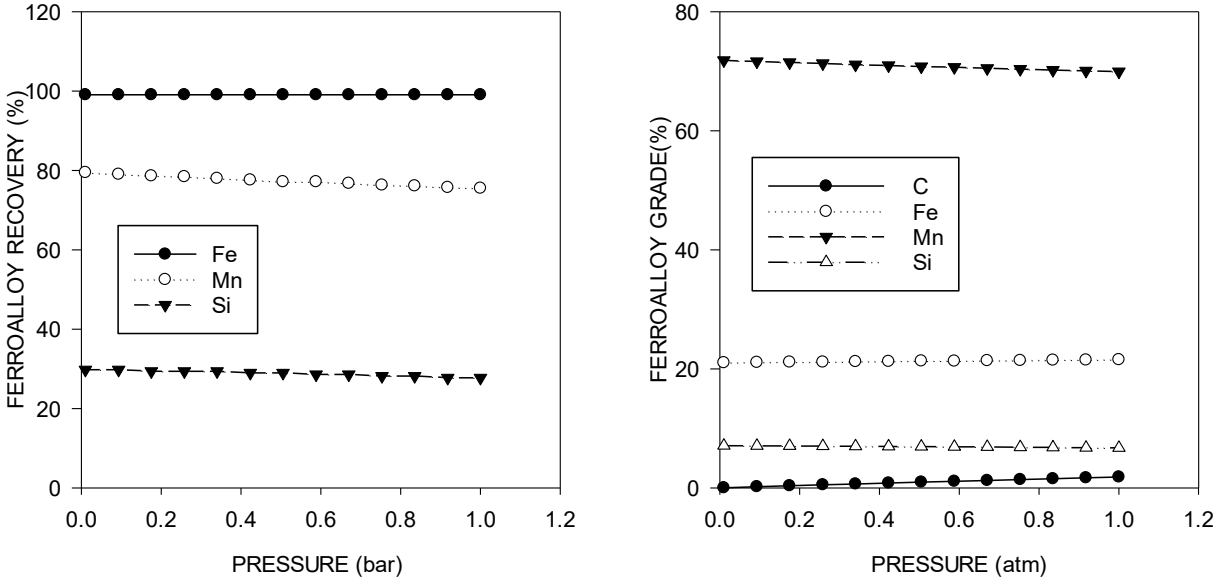

Figure 11 Effect of atmospheric pressure on (a) the recovery of the value metals to Alloy 2 and (b) the grade of Alloy II.

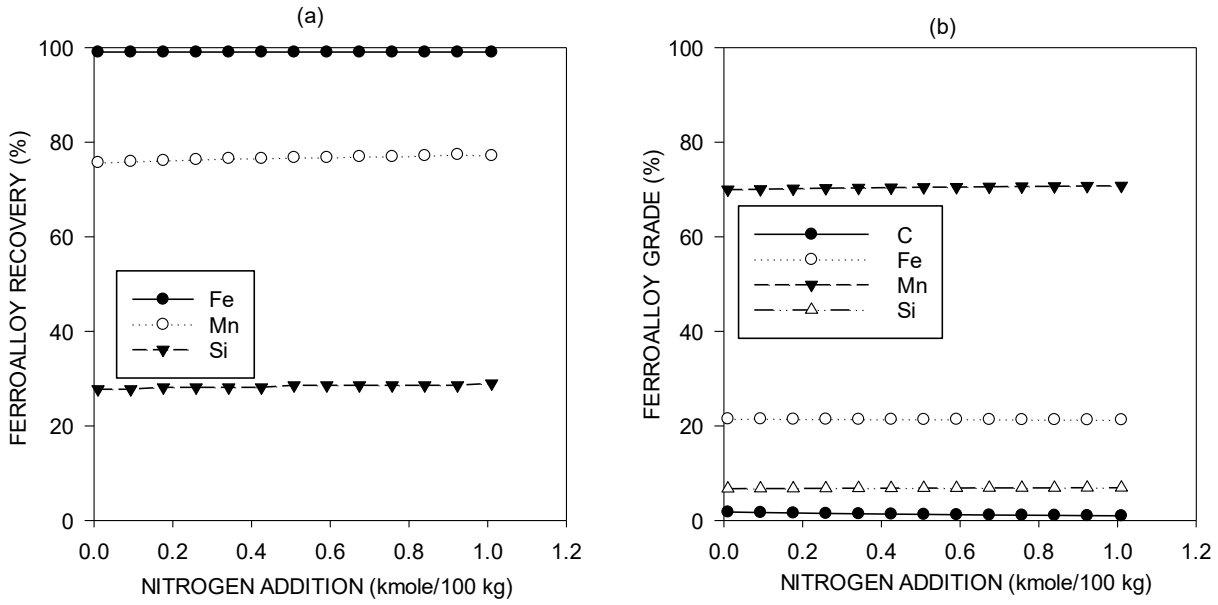

Figure 12 Effect of nitrogen additions on (a) the recovery of the value metals to Alloy 2 and (b) the grade of Alloy II.

As for the low-temperature Stage I reduction process for Alloy I, the effect of nodule composition was also investigated for Stage II for the production of Alloy II. Figures 13(a)–(e) show the effects of additional CaO, MgO, SiO_2, Fe_2O_3 and Al_2O_3, respectively, on the equilibrium amounts of carbon, iron, manganese and silicon in Alloy II. For SiO_2, the major effects are a reduction in the amount of manganese and an increase in the amount of silicon, while the amounts of iron and carbon remain relatively constant. This reflects the enhanced reduction of SiO_2, which consumes carbon, and thus there is less carbon available for the reduction of MnO. Consequently, increasing SiO_2 additions promote silicon recovery at the expense of manganese recovery. For CaO there is an increase in both the amount of manganese and carbon, together with a decrease in the amount of silicon, while the amount of iron remains relatively constant. Here, increasing lime results in the formation of more stable silicates, which hinders the reduction of SiO_2 and thus more carbon becomes available for the reduction of MnO. As a result, manganese recovery is enhanced while silicon recovery is suppressed.

Al_2O_3 behaves in a similar but less pronounced manner, forming stable aluminosilicates, and thus the manganese and carbon amounts increase, while the silicon amount decreases and the amount of iron remains essentially constant. The smaller effect of Al_2O_3 compared with lime indicates that aluminosilicate formation has a weaker influence on the equilibrium distribution of manganese and silicon. For MgO, there are only slight increases in the manganese and carbon contents, while the silicon amount decreases somewhat and the iron content remains constant. MgO behaves in a similar manner to lime but the effect is less pronounced. Fe_2O_3 has the most significant effect of the five oxides investigated, as it is the least stable and promotes more oxidizing conditions. With increasing amounts of Fe_2O_3 in the nodules, the amount of iron in the alloy increases. On the other hand, due to the increase in the oxidizing conditions, the amounts of manganese, silicon and carbon decrease. Among the gangue components investigated, Fe_2O_3 therefore has the greatest influence on the equilibrium alloy composition because it directly increases the oxygen potential of the system and consequently suppresses the reduction of MnO and SiO_2.

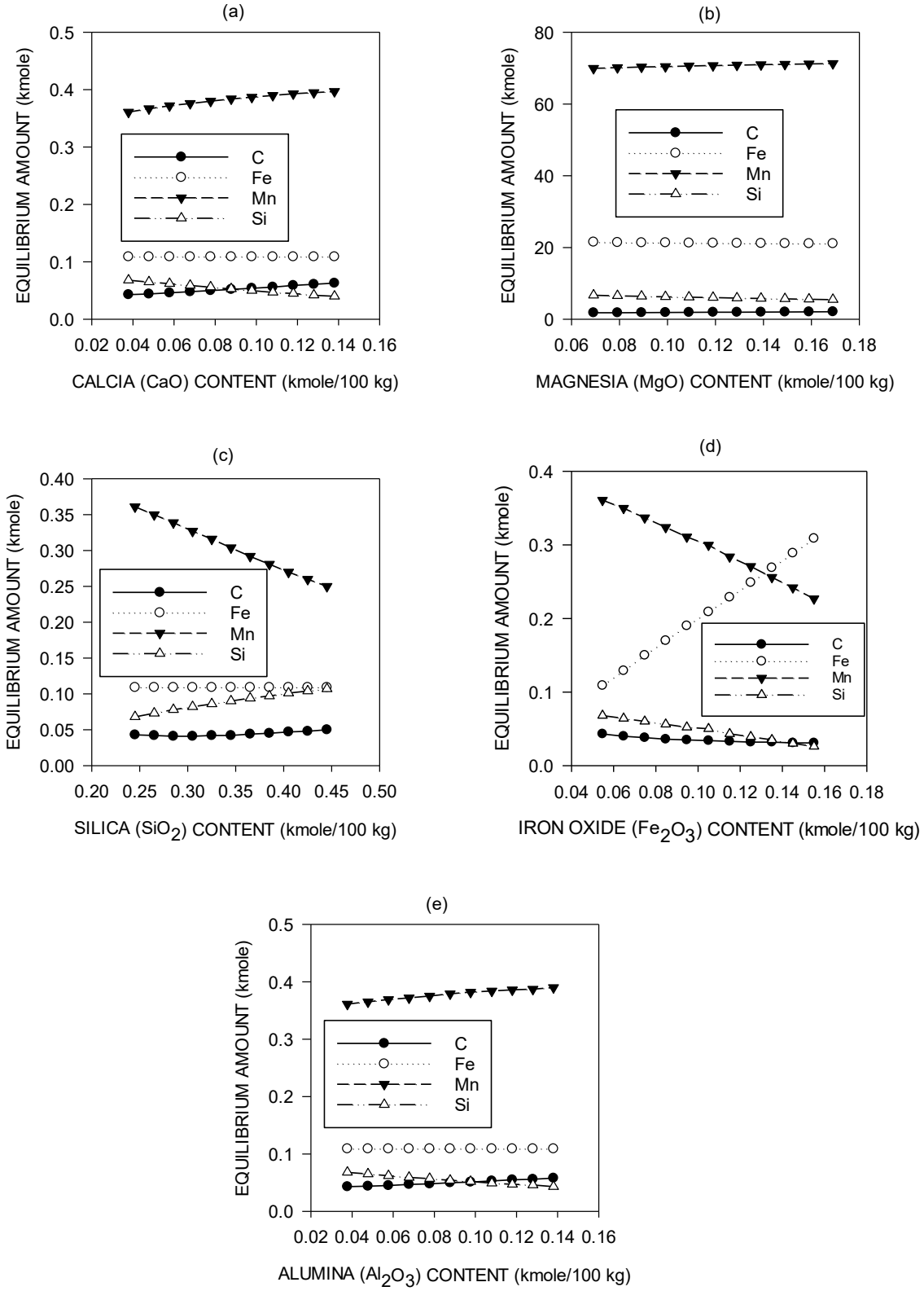

Figure 13 Carbon, iron, manganese and silicon equilibrium amounts in Alloy II as a function of (a) lime, (b) magnesia, (c) silica, (d) hematite and (e) alumina amounts for a carbon addition of 1.12 kmole/100 kg at 1600 °C.

3.4 Comparison with Experimental Observations

Published work on manganese-rich nodule slags and residues provides a useful basis for comparison with the Stage II calculations. The systems differ in feed composition, flux additions, reductant dosage and target alloy composition, and therefore exact agreement is not expected. In the present calculations, at 1600 °C and 1.12 kmole C/100 kg, Mn recovery is approximately 75% and the alloy contains about 70% Mn, 22% Fe, 6.7% C and 1.8% Si. Increasing the carbon addition to 1.62 kmole C/100 kg raises Mn and Si recoveries to approximately 98% and 56%, respectively, and produces an alloy containing approximately 69% Mn, 16.3% Fe, 10.2% Si and 5% C. High-temperature treatment of manganese-rich nodule slag has previously produced ferromanganese, supporting further processing of the Mn-rich residue after recovery of the non-ferrous metals [1]. Quantitatively, Mn recovery above 77% has been reported from manganese-rich nodule residue [36], compared with approximately 75% predicted here at 1600 °C and 1.12 kmole C/100 kg. Silicomanganese production from a nodule-derived feed at approximately 1650 °C yielded an alloy containing 69.6 wt.% Mn [37], which is close to the predicted value of approximately 69 wt.% Mn at 1600 °C and 1.62 kmole C/100 kg. The larger differences in Si, Fe and C contents are reasonable considering the differences in charge composition and targeted alloy product. Previous smelting studies also show a strong influence of reductant addition and slag composition on manganese recovery and alloy formation[1,36,37]. This agrees with the calculated increase in Mn and Si recoveries with carbon addition and their sensitivity to SiO_2 and basic oxide contents. Differences between calculated and measured values can also arise from kinetics, residence time, mass transfer, slag properties and metal–slag separation, which are not considered in the equilibrium model. Despite these differences, the calculated temperature range, Mn recovery and alloy Mn content are comparable with values achieved experimentally.

Table 2 Comparison of Stage II predictions with experimental manganese-alloy production.

Experimental conditions and observations	Present thermodynamic prediction	Comparison	Study
• Mn-rich nodule slag reduced at 1500 °C • Most alloys contained >78 wt.% Mn • Si generally <1.2 wt.% • 5–15 wt.% CaO provided suitable results	• High Mn recovery requires 1600 °C • At 1.12 kmole C/100 kg: 70% Mn and 1.8% Si • Slag composition strongly affects Mn and Si recovery	• Same high-temperature Stage II regime • Confirms the importance of slag chemistry in ferromanganese production	[1]
• Silicomanganese produced from leached nodule residue blended with Mn ore • Residue contained 26% Mn, 10% Fe and 6% SiO_2 • Mn recovery: >77%	• At 1600 °C and 1.12 kmole C/100 kg • Mn recovery: 75%	• Mn recovery: >77 vs 75% • Close quantitative similarity despite different feed and operating conditions	[36]
• Nodule-derived Mn-silicate feed reduced at 1650 °C • Alloy: 69.6% Mn, 18.1% Si, 10.7% Fe and 1–2% C	• At 1600 °C and 1.62 kmole C/100 kg • Alloy: 69% Mn, 10.2% Si, 16.3% Fe and 5% C	• Temperature: 1650 vs 1600 °C • Mn: 69.6 vs 69 wt.% • Differences in Si, Fe and C reflect different feed formulation and target alloy	[37]
• Carbothermic smelting at 1350 °C • Graphite addition and MnO/SiO_2 ratio strongly affected reduction and metal–slag separation • Mn-rich slag was retained for subsequent Mn recovery	• Increasing carbon strongly increases Mn and Si recovery • Increasing SiO_2 favours Si recovery but decreases Mn recovery	• Same strong dependence on reductant addition and slag composition • Direct numerical comparison is limited by different processing objectives	[38]

4 CONCLUSIONS

1- This study established the thermodynamic operating window for converting the manganese-rich residue remaining after selective recovery of critical battery metals into a ferromanganese–silicide alloy. Using HSC Chemistry® 7.1, the equilibrium conditions governing the second stage of the proposed two-stage selective carbothermic process were determined. Thermodynamic calculations showed that MnO is substantially more stable than the oxides of Cu, Ni and Co reduced during the first stage of the process and therefore requires significantly higher reduction temperatures.

2- The thermodynamic calculations showed that temperatures above approximately 1600 °C, together with hyperstoichiometric carbon addition above the stoichiometric requirement for manganese and iron reduction, are necessary to achieve high recoveries of manganese while simultaneously reducing the remaining FeO and partially reducing the SiO_2. The additional carbon requirement arises because carbon is consumed not only in the reduction of MnO, but also in the reduction of SiO_2 and the formation of carbide and silicide phases within the ferroalloy.

3- For the stoichiometric carbon addition of 1.12 kmole C per 100 kg of nodules, the predicted ferromanganese–silicide alloy composition at 1600 °C was approximately 70% Mn, 22% Fe, 6.7% C and 1.8% Si, although the manganese recovery was limited to approximately 75%. Increasing the carbon addition to 1.62 kmole C per 100 kg increased the manganese recovery to approximately 98% and the silicon recovery to approximately 56%, producing a ferromanganese–silicide alloy containing approximately 69% Mn, 16.3% Fe, 10.2% Si and 5% C. Beyond approximately 1.55 kmole C per 100 kg, further carbon addition produced only minor changes in both the equilibrium recoveries and alloy composition. Higher silicon contents required progressively higher reduction temperatures.

4- As observed for the first reduction stage, variations in atmospheric pressure and nitrogen content had only a limited influence on metal recoveries because carbon monoxide remained the dominant gaseous species throughout the reduction process. Consequently, significant reductions in pressure or large nitrogen additions produced only modest improvements in equilibrium metal recoveries and are therefore unlikely to provide significant practical advantages for ferromanganese–silicide alloy production.

5- Gangue composition influenced the reduction behaviour primarily through the formation of stable silicate phases. SiO_2 additions reduced manganese recovery while increasing silicon recovery to the alloy, whereas CaO and Al_2O_3 promoted manganese recovery but reduced silicon recovery. MgO produced only a slight increase in manganese recovery, while additional Fe_2O_3 increased iron recovery but decreased the recoveries of manganese, silicon and carbon. Among the gangue components investigated, Fe_2O_3 had the greatest influence on the equilibrium alloy composition by increasing the oxygen potential of the system.

6- The second stage converts the manganese-rich Stage I residue into a ferromanganese–silicide alloy, completing the proposed two-stage recovery strategy. Published experiments support the

predicted high-temperature operating region, with reported Mn recovery above 77% compared with approximately 75% predicted here, and an experimental alloy containing 69.6 wt.% Mn compared with approximately 69 wt.% predicted in the present study.

5 Acknowledgements

The authors thank the Natural Sciences and Engineering Research Council of Canada (NSERC) for their support of this research.

6 References

[1] M. Sommerfeld, D. Friedmann, T. Kuhn, B. Friedrich, "Zero-Waste": A Sustainable Approach on Pyrometallurgical Processing of Manganese Nodule Slags, Minerals 8 (2018) 544. https://doi.org/10.3390/min8120544.

[2] J.R. Hein, A. Koschinsky, T. Kuhn, Deep-ocean polymetallic nodules as a resource for critical materials, Nat Rev Earth Environ 1 (2020) 158–169. https://doi.org/10.1038/s43017-020-0027-0.

[3] D. Paulikas, S. Katona, E. Ilves, S.H. Ali, Life cycle climate change impacts of producing battery metals from land ores versus deep-sea polymetallic nodules, Journal of Cleaner Production 275 (2020) 123822. https://doi.org/10.1016/j.jclepro.2020.123822.

[4] N.S. Randhawa, J. Hait, R.K. Jana, A brief overview on manganese nodules processing signifying the detail in the Indian context highlighting the international scenario, Hydrometallurgy 165 (2016) 166–181. https://doi.org/10.1016/j.hydromet.2015.09.013.

[5] W. Zhang, C.Y. Cheng, Manganese metallurgy review. Part I: Leaching of ores/secondary materials and recovery of electrolytic/chemical manganese dioxide, Hydrometallurgy 89 (2007) 137–159. https://doi.org/10.1016/j.hydromet.2007.08.010.

[6] J. Ju, Y. Feng, H. Li, Z. Xue, R. Ma, Y. Li, Research advances, challenges and perspectives for recovering valuable metals from deep-sea ferromanganese minerals: A comprehensive review, Separation and Purification Technology 315 (2023) 123626. https://doi.org/10.1016/j.seppur.2023.123626.

[7] R.S.B. Elliott, Reduction of Manganese Ore by Methane, University of Toronto, 2023. http://hdl.handle.net/1807/130435 (accessed August 3, 2026).

[8] R.H. Eric, Chapter 1.12 - Production of Ferroalloys, in: S. Seetharaman, R. Guthrie, A. McLean, S. Seetharaman, H.Y. Sohn (Eds.), Treatise on Process Metallurgy (Second Edition), Elsevier, 2024: pp. 415–453. https://doi.org/10.1016/B978-0-323-85373-6.00020-X.

[9] A. Cheraghi, H. Yoozbashizadeh, E. Ringdalen, J. Safarian, Kinetics and Mechanism of Low-Grade Manganese Ore Reduction by Natural Gas, Metall Mater Trans B 50 (2019) 1566–1580. https://doi.org/10.1007/s11663-019-01574-4.

[10] C.A. Pickles, O. Marzoughi, Thermodynamic modelling of decomposition processes in the Mn-O and Mn-O-H systems, Canadian Metallurgical Quarterly 62 (2023) 151–170. https://doi.org/10.1080/00084433.2022.2060602.

[11] K. Su, X. Ma, J. Parianos, B. Zhao, Thermodynamic and Experimental Study on Efficient Extraction of Valuable Metals from Polymetallic Nodules, Minerals 10 (2020) 360. https://doi.org/10.3390/min10040360.

[12] H. Cengizler, R.H. Eric, Silicon and Manganese Partition Between Slag and Metal Phases and Their Activities Pertinent to Ferromanganese and Silicomanganese Production, in: R.G. Reddy, P. Chaubal, P.C. Pistorius, U. Pal (Eds.), Advances in Molten Slags, Fluxes, and Salts: Proceedings of the 10th International Conference on Molten Slags, Fluxes and Salts 2016, Springer International Publishing, Cham, 2016: pp. 1309–1317. https://doi.org/10.1007/978-3-319-48769-4_142.

[13] D. Friedmann, A.K. Pophanken, B. Friedrich, Pyrometallurgical Treatment of High Manganese Containing Deep Sea Nodules, J. Sustain. Metall. 3 (2017) 219–229. https://doi.org/10.1007/s40831-016-0070-8.

[14] T. Abramovski, V. Stefanova, R. Causse, A. Romanchuk, Technologies For the Processing Of Polymetallic Nodules from Clarion Clipperton Zone In the Pacific Ocean, in: 2017. https://www.semanticscholar.org/paper/TECHNOLOGIES-FOR-THE-PROCESSING-OF-POLYMETALLIC-IN-Abramovski-Stefanova/891fda80ae55c9adb5020432e25c2931b073a01b (accessed August 3, 2026).

[15] F. Zhao, X. Jiang, S. Wang, L. Feng, D. Li, The Recovery of Valuable Metals from Ocean Polymetallic Nodules Using Solid-State Metalized Reduction Technology, Minerals 10 (2020) 20. https://doi.org/10.3390/min10010020.

[16] J. Ju, Y. Feng, H. Li, R. Ma, Y. Li, H. Zhao, H. Wang, S. Jiang, An innovative method for the efficient and selective extraction of Co, Ni, Cu, and Mn from oceanic cobalt-rich crusts by ammonium sulfate roasting: Behavior, roasting kinetics and mechanism, Minerals Engineering 207 (2024) 108543. https://doi.org/10.1016/j.mineng.2023.108543.

[17] U. Manzoor, T. Lüttke, D. Raabe, I.R. Souza Filho, Low-waste, single-step, sustainable extraction of critical metals from deep-sea polymetallic nodules, Sci Adv 11 (2025) eaea1223. https://doi.org/10.1126/sciadv.aea1223.

[18] O. Marzoughi, R. Verge, S. Annan, R.M. Hutcheon, J. Donald, C.A. Pickles, Characterization, permittivities and drying kinetics during microwave dewatering of deep-sea polymetallic nodules, Chemical Engineering Journal Advances 26 (2026) 101102. https://doi.org/10.1016/j.ceja.2026.101102.

[19] S. Wang, X. Liu, J. Wang, K. Cui, H. Liu, J. Qiu, W. Zhou, Advances in iron-manganese separation from ferromanganese ores: Technologies, challenges, and future trends, Powder Technology 484 (2026) 123006. https://doi.org/10.1016/j.powtec.2026.123006.

[20] O. Marzoughi, J. Forster, J. Donald, C.A. Pickles, Microwave dewatering of deep-sea polymetallic nodules: Bench-scale and pilot-scale studies, Minerals Engineering 235 (2026) 109879. https://doi.org/10.1016/j.mineng.2025.109879.

[21] M.J. Lindstrom-Parkins, R. Elliott, M. Fong, C. Lee, Review of Polymetallic Sea Nodules and Their Processing Routes, in: Ni-Co 2025, 6th International Symposium on Nickel and Cobalt, Springer Nature Switzerland, Cham, 2025: pp. 779–795. https://doi.org/10.1007/978-3-032-00167-2_59.

[22] T. Kohga, M. Imamura, J. Takahashi, N. Tanaka, T. Nishizawa, Recovering iron, manganese, copper, cobalt, and high-purity nickel from sea nodules, JOM 47 (1995) 40–43. https://doi.org/10.1007/BF03221339.

[23] B. Ma, P. Xing, W. Yang, C. Wang, Y. Chen, H. Wang, Solid-State Metalized Reduction of Magnesium-Rich Low-Nickel Oxide Ores Using Coal as the Reductant Based on Thermodynamic Analysis, Metall Mater Trans B 48 (2017) 2037–2046. https://doi.org/10.1007/s11663-017-0977-x.

[24] O.K. Brustad, J. Låstad, A. Hoseinpur, J. Safarian, Characterization, Calcination and Pre-Reduction of Polymetallic Manganese Nodules by Hydrogen and Methane, Metals 12 (2022) 2013. https://doi.org/10.3390/met12122013.

[25] X. Deng, D. He, R. Chi, C. Xiao, J. Hu, The Reduction Behavior of Ocean Manganese Nodules by Pyrolysis Technology Using Sawdust as the Reductant, Minerals 10 (2020) 850. https://doi.org/10.3390/min10100850.

[26] J. Li, Y. Hu, L. Yue, L. Zeng, S. Wu, M. Wang, W. Guan, Z. Cao, Q. Li, G. Zhang, Recovery of critical battery metals from cobalt-rich deep-sea polymetallic nodules: Selective carbothermal reduction based on kinetics, Journal of Environmental Chemical Engineering 12 (2024) 111631. https://doi.org/10.1016/j.jece.2023.111631.

[27] Y. Okajima, Process for treating manganese nodules, US4029498A, 1977. https://patents.google.com/patent/US4029498A/en (accessed August 3, 2026).

[28] N. Anacleto, O. Ostrovski, S. Ganguly, Reduction of Manganese Ores by Methane-containing Gas, ISIJ International 44 (2004) 1615–1622. https://doi.org/10.2355/isijinternational.44.1615.

[29] O. Ostrovski, N. Anacleto, S. Ganguly, Reduction of Manganese Ores by Methane-Containing Gas, in: Transformation Through Technology, Cape Town, South Africa, 2004.

[30] T.A. Larssen, M. Tangstad, I.T. Kero, Gaseous Reduction of Mn Ores in CO-CO2 Atmosphere, in: B.R. Davis, M.S. Moats, S. Wang, D. Gregurek, J. Kapusta, T.P. Battle, M.E. Schlesinger, G.R. Alvear Flores, E. Jak, G. Goodall, M.L. Free, E. Asselin, A. Chagnes, D. Dreisinger, M. Jeffrey, J. Lee, G. Miller, J. Petersen, V.S.T. Ciminelli, Q. Xu, R. Molnar, J. Adams, W. Liu, N. Verbaan, J. Goode, I.M. London, G. Azimi, A. Forstner, R. Kappes, T. Bhambhani (Eds.), Extraction 2018, Springer International Publishing, Cham, 2018: pp. 1093–1101. https://doi.org/10.1007/978-3-319-95022-8_88.

[31] P. Mu, J. Zhao, X. Zhang, C. Yang, J. Wu, Y. Yang, Y. Tang, M. Xiao, M. Pan, H. Zhao, G. Fang, G. Jiang, Z. Tan, D. Pan, Research progress in preparation of manganese-based materials from multisource manganese ores, Green and Smart Mining Engineering 2 (2025) 483–514. https://doi.org/10.1016/j.gsme.2025.05.010.

[32] F. Li, S. Xu, J. Qiu, Z. Chen, W. Du, D. Ju, K. Xie, Optimization of Gas–Solid Co-Reduction Conditions for Deep-Sea Polymetallic Nodules, JOM 75 (2023) 5718–5728. https://doi.org/10.1007/s11837-023-06181-y.

[33] R. Elliott, K. Coley, S. Mostaghel, M. Barati, Review of Manganese Processing for Production of TRIP/TWIP Steels, Part 2: Reduction Studies, JOM 70 (2018) 691–699. https://doi.org/10.1007/s11837-018-2773-8.

[34] F. Li, S. Xu, D. Zhou, D. Ju, W. Du, H. Wang, Optimized Conditions for Extracting Fe–Ni–Co–Cu Alloy from Polymetallic Nodules, J. Sustain. Metall. 9 (2023) 1363–1377. https://doi.org/10.1007/s40831-023-00732-y.

[35] C.A. Pickles, O. Marzoughi, Thermodynamic analysis of metal speciation during the chlorosulphation of electric arc furnace dust, Minerals Engineering 140 (2019) 105874. https://doi.org/10.1016/j.mineng.2019.105874.

[36] N.S. Randhawa, R.K. Jana, N.N. Das, Silicomanganese production utilising low grade manganese nodules leaching residue, Mineral Processing and Extractive Metallurgy 122 (2013) 6–14. https://doi.org/10.1179/1743285512Y.0000000022.

[37] M.N. Boulby, K. Bradley, J.R. Donald, Production of Battery-Grade Sulfates from Deep-Sea Polymetallic Nodules, in: Metallurgy and Materials Society of CIM (Ed.), Proceedings of the 63rd Conference of Metallurgists, COM 2024, Springer Nature Switzerland, Cham, 2025: pp. 1265–1275. https://doi.org/10.1007/978-3-031-67398-6_211.

[38] K. Su, X. Ma, J. Parianos, B. Zhao, Thermodynamic and Experimental Study on Efficient Extraction of Valuable Metals from Polymetallic Nodules, Minerals 10 (2020) 360. https://doi.org/10.3390/min10040360.